arXiv:quant-ph/0607007v1 2 Jul 2006

Geometric quantum computation using fictitious spin-1/2 subspaces of strongly dipolar coupled nuclear spins

T. Gopinath and Anil Kumar*

NMR Quantum Computing and Quantum Information Group.
Department of Physics, and NMR Research Centre.
Indian Institute of Science, Bangalore - 560012, India.

Geometric phases have been used in NMR, to implement controlled phase shift gates for quantum information processing, only in weakly coupled systems in which the individual spins can be identified as qubits. In this work, we implement controlled phase shift gates in strongly coupled systems, by using non-adiabatic geometric phases, obtained by evolving the magnetization of fictitious spin-1/2 subspaces, over a closed loop on the Bloch sphere. The dynamical phase accumulated during the evolution of the subspaces, is refocused by a spin echo pulse sequence and by setting the delay of transition selective pulses such that the evolution under the homonuclear coupling makes a complete 2π rotation. A detailed theoretical explanation of non-adiabatic geometric phases in NMR is given, by using single transition operators. Controlled phase shift gates, two qubit Deutsch-Jozsa algorithm and parity algorithm in a qubit-qutrit system have been implemented in various strongly dipolar coupled systems obtained by orienting the molecules in liquid crystal media.

I. INTRODUCTION

The concept of using quantum systems for information processing was first introduced by Benioff [1]. In 1985 Deutsch described quantum computers which exploit the superposition of multi particle states, thereby achieving massive parallelism [2]. Researchers have also studied the possibility of solving certain types of problems more efficiently than can be done on conventional computers [2, 3, 4, 5]. Quantum computing and quantum information processing, requires the ability to execute conditional dynamics between two qubits [6]. Several techniques are being exploited including nuclear magnetic resonance [7, 8, 9, 10, 11]. The experimental realization has been limited by many factors, such as decoherence, difficulty in achieving higher number of qubits and controlled manipulation of qubits with higher fidelity [12, 13, 14, 15, 16, 17]. A recent development in this field is to use geometric phases to build fault tolerant controlled phase shift gates [18].

---

* Electronic mail: anilnmr@physics.iisc.ernet.in

Berry's discovery of geometric phase [19] accompanying cyclic adiabatic evolution has triggered an immense effects in holonomy effects in quantum mechanics and has led to many generalizations. Simon[20] explained that this geometric phase could be viewed as a consequence of parallel transport in a curved space appropriate to the quantum system. In nuclear magnetic resonance, geometric phase was first verified by Pines et.al. in adiabatic regime [21]. A similar approach was used by Jones, to implement controlled phase shift gates by geometric phases in a two qubit system formed by a weak J coupling [22, 23]. However the adiabatic condition is not satisfied in many realistic cases because of the long operation time [24] . Hence it is difficult to experimentally realize quantum computation with adiabatic evolutions, particularly for systems having short decoherence time. To overcome this disadvantage, it was proposed to use the non-adiabatic cyclic geometric phase (Aharonov and Anandan phase [26]) to construct geometric quantum gates [25]. These gates not only have faster gate operation time, but also have intrinsic features of the geometric phase, and hence robust against certain types of operational errors [24, 25]. For a non-adiabatic cyclic evolution, the total phase difference between the initial and final states, consists of both the geometric and dynamical phases. Therefore, to obtain only the non-adiabatic geometric phase, one has to remove the dynamical component. Non-adiabatic geometric phase in NMR was also first verified by Pines et.al [27]. Non adiabatic geometric phases in NMR, were used to implement controlled phase shift gates, Deutsch-Jozsa (DJ) and Grover algorithms in a two qubit system formed by weak J coupling [28].

Most of the NMR Quantum information processing (QIP) experiments have utilized systems having indirect spin-spin couplings (scalar J couplings) [7, 8, 9, 10, 29]. Since these couplings are mediated via the covalent bonds, the number of coupled spins and hence the number of qubits is limited to a few qubits [11]. Another approach is to use direct dipole-dipole couplings between the spins which are larger in magnitude [30, 31, 33, 36, 37, 38]. In liquids the dipolar couplings are averaged to zero due to rapid isotropic reorientations of the molecules and in rigid solids there are too many couplings yielding broad lines[39]. In molecules partially oriented in anisotropic media, like liquid crystals, one obtains partially averaged intra molecular dipolar couplings with only a finite number of dipolar coupled spins, yielding finite number of sharp NMR resonances [30]. However in such cases often the dipolar couplings are large or comparable to chemical shifts differences between the coupled spins, leading to spins becoming strongly coupled. The method of spin selective pulses and J evolution used in NMR-QIP of weakly coupled spins (liquid state NMR-QIP), leads to complications in strongly coupled spins because of the non secular terms in the Hamiltonian. Therefore such systems have been utilized for quantum information processing, by using transition selective pulses and treating the 2^n non-degenerate energy levels as an "n" qubit system. Preparation of pseudopure states, one qubit DJ algorithm and quantum gates which do not need control of phases, have been implemented in such systems using transition selective pulses [30, 31, 33]. Recently an 8 and a 12 qubit systems have been achieved using dipolar coupled spins in molecules oriented in liquid crystals [34, 35].

In this paper, we implement controlled phase shift gates, two qubit DJ algorithm and the parity algorithm in strongly dipolar coupled spins, by using non-adiabatic geometric phases, obtained by evolving the magnetization of fictitious spin-1/2 subspaces (formed by pairs of energy levels). This method requires efficient transition selective pulses and refocusing of Hamiltonian evolution. The physical systems chosen, contain a single non secular term $\vec{I_i}.\vec{I_j}$ in the homonuclear dipolar Hamiltonian $D_{ij}(3I_{zi}I_{zj} - \vec{I_i}.\vec{I_j})$, which is refocused by setting the delay of a transition selective pulse such that the evolution due to the coupling makes a complete 2π rotation. To the best of our knowledge, this is the first implementation of quantum algorithms in strongly coupled nuclear spins by using geometric phases.

In section(II), we outline the non-adiabatic Geometric phases by using both, Bloch sphere approach and single transition operators [40]. In section(III), we describe the implementation of controlled phase shift gates in $^{13}CH_3I$ partially oriented in ZLI-1132 liquid crystal. In section(IV) two qubit DJ algorithm is implemented in dipolar coupled equivalent protons of oriented CH_3CN. In section (V) parity algorithm is implemented in a qubit-qutrit system of CH_2FCN partially oriented in ZLI-1132, and the results are concluded in section(VI).

II. NON-ADIABATIC GEOMETRIC PHASES IN NMR

In order to describe the non-adiabatic geometric phases in NMR, we discuss the evolution of the magnetization of single quantum transitions, under transition selective pulses, using the approach of single transition operator algebra [40], briefly outlined below.

Consider a 4 level system (fig.1a), consisting of 6 pairs (r,s) of energy levels (r=1,2,3, and r $<$ s $\leq$ 4). Each pair of energy levels can be considered as belonging to a fictitious spin-1/2 subspace (virtual two level system), and the dynamics of the magnetization of the system can be explained by using single transition operators [40]. Here we assume that the single quantum magnetization of the subspaces (1,2), (2,3) and (3,4), is directly observable, hence one can easily manipulate those subspaces. The angular momentum operators (single transition Cartesian operators) $I_\alpha^{(r,s)}$ (α=x,y,z) have been defined as [40],

$$\begin{aligned}
\langle i|I_x^{(r,s)}|j\rangle &= \frac{1}{2}(\delta_{ir}\delta_{js} + \delta_{is}\delta_{jr}),\\
\langle i|I_y^{(r,s)}|j\rangle &= \frac{i}{2}(-\delta_{ir}\delta_{js} + \delta_{is}\delta_{jr}),\\
\langle i|I_z^{(r,s)}|j\rangle &= \frac{1}{2}(\delta_{ir}\delta_{jr} - \delta_{is}\delta_{js}),
\end{aligned} \tag{1}$$

where i, j = 1, 2, 3 and 4. From this definition it follows that [40],

$$I_x^{(r,s)} = I_x^{(s,r)}, \quad I_y^{(r,s)} = -I_y^{(s,r)} \ \ and \ \ I_z^{(r,s)} = -I_z^{(s,r)}. \tag{2}$$

In the following, geometric phases are explained by using Bloch sphere approach [23]. Later, we describe the commutation relations of single transition operators eqn.(1), and show that geometric phases can be obtained by using pair of transition selective π pulses, with suitable phases in the xy plane. The removal of dynamical phase (phase acquired due to internal Hamiltonian evolution) is discussed in sections III, IV and V.

From equation (1), one can see that, the angular momentum operators of (r,s) subspace, after removing rows and columns containing zeroes, are Pauli spin matrices and hence the basis states of (r,s) subspace can be considered as $|0\rangle$ and $|1\rangle$, which can be represented on a Bloch sphere fig.(1b). In this paper we follow the convention [17] that the lower state 'r', in the (r,s) subspace, represents $|0\rangle$ and the upper state 's' represents $|1\rangle$. In general, every two level sub-system at equilibrium, can be considered to be in a pseudopure state [41, 42]. Hence the (r,s) subsystem can be considered as in the pseudopure state $|0\rangle$. In such systems, to encode the phase information, we create initial states, consisting of superposition states, in each of the subspaces (1,2), (2,3) and (3,4), given by,

$$|\psi_{rs}\rangle = \frac{1}{\sqrt{2}}(|0\rangle + |1\rangle)_{rs}, \qquad where \quad r = 1, 2, 3 \;\; and \;\; s = r + 1. \tag{3}$$

The state of (r,s) subspace, $|\psi_{rs}\rangle$ (eqn.3), consist of coherences $I_x^{(r,s)}$ (r=1,2 and 3, s=r+1), which can be created experimentally by applying a $(\pi/2)_y$ pulse on the equilibrium state of the whole system. The coherence $I_x^{(r,s)}$ can in general be written as,

$$I_x^{(r,s)} = |\psi_{rs}\rangle\langle\psi_{rs}| - \frac{1}{2}I^{(r,s)}, \tag{4}$$

where $I^{(r,s)}$ is the identity matrix of (r,s) subspace and $|\psi_{rs}\rangle\langle\psi_{rs}|$ represents the density matrix $\sigma_{(r,s)}$. Since the identity matrix does not contribute to NMR signal, the density matrix $\sigma_{(r,s)} = |\psi_{rs}\rangle\langle\psi_{rs}|$ represents $I_x^{(r,s)}$ and vice versa.

The state $|\psi_{rs}\rangle$, can be manipulated, such that it goes through a closed loop on the Bloch sphere, thereby acquiring a geometric phase (fig.1b). The geometric phase acquired is respectively $e^{i\Omega/2}$ and $e^{-i\Omega/2}$ for the states $|0\rangle$ and $|1\rangle$, where Ω is the solid angle subtended by the closed loop at the center of the Bloch sphere (fig.1b) [23, 27]. The unitary operator for the above operation is a phase shift gate, given for example, for the (2,3) subspace as,

$$U(2,3) = \begin{pmatrix} 1 & 0 & 0 & 0 \\ 0 & e^{i\Omega/2} & 0 & 0 \\ 0 & 0 & e^{-i\Omega/2} & 0 \\ 0 & 0 & 0 & 1 \end{pmatrix}. \tag{5}$$

The state $|\psi_{rs}\rangle$, under the above unitary operator U(2,3), is transformed to $|\psi'_{rs}\rangle$, given by,

$$\begin{aligned} |\psi'_{12}\rangle &= \frac{1}{\sqrt{2}}(|0\rangle + e^{i\Omega/2}|1\rangle)_{12} \\ |\psi'_{23}\rangle &= \frac{1}{\sqrt{2}}(e^{i\Omega/2}|0\rangle + e^{-i\Omega/2}|1\rangle)_{23} \\ |\psi'_{34}\rangle &= \frac{1}{\sqrt{2}}(e^{-i\Omega/2}|0\rangle + |1\rangle)_{34}. \end{aligned} \tag{6}$$

The states $|\psi'_{rs}\rangle$, in eqn.6, can be written in the density matrix form $[\sigma'_{rs} = |\psi'_{rs}\rangle\langle\psi'_{rs}|]$, as,

$$\sigma'_{12} = \frac{1}{2}\begin{pmatrix} 1 & e^{-i\Omega/2} \\ e^{i\Omega/2} & 1 \end{pmatrix}, \quad \sigma'_{23} = \frac{1}{2}\begin{pmatrix} 1 & e^{i\Omega} \\ e^{-i\Omega} & 1 \end{pmatrix}, \quad and \;\; \sigma'_{34} = \frac{1}{2}\begin{pmatrix} 1 & e^{-i\Omega/2} \\ e^{i\Omega/2} & 1 \end{pmatrix}. \tag{7}$$

In the following we show that, the geometric phase gate U(2,3) can be obtained by, cyclic evolution of $I_x^{(2,3)}$ (state $|\psi_{23}\rangle$), by means of selective π pulses on transition (2,3).

The effect of transition selective pulses can be explained by using the commutators of single transition operators given in eqn.(1). If the coherence and the r.f. pulse involves the same transition, then the transformation follows the usual commutation relation [40],

$$[I_\alpha^{(r,s)}, I_\beta^{(r,s)}] = iI_\gamma^{(r,s)}, \tag{8}$$

where (α, β, γ) is a cyclic permutation of (x,y,z).

The commutator in eqn.8, implies the property that [39],

$$e^{-i\theta I_\gamma^{(r,s)}} I_\alpha^{(r,s)} e^{i\theta I_\gamma^{(r,s)}} = I_\alpha^{(r,s)} cos(\theta) + I_\beta^{(r,s)} sin(\theta), \tag{9}$$

which can be interpreted as, rotation of $I_\alpha^{(r,s)}$ towards $I_\beta^{(r,s)}$, around the γ axis of (r,s) subspace.

If the pulse is applied on the transition (r,s), and a connected transition (t,r) is observed, then the commutation relations become [40],

$$\begin{aligned} &[I_x^{(t,r)}, I_x^{(t,s)}] = \frac{i}{2} I_y^{(r,s)} \\ and \quad &[I_y^{(t,r)}, I_x^{(t,s)}] = \frac{i}{2} I_x^{(r,s)}. \end{aligned} \tag{10}$$

The commutator relations of eqn.(10) imply that:

$$\begin{aligned} &e^{-i\theta I_y^{(r,s)}} I_x^{(t,r)} e^{i\theta I_y^{(r,s)}} = I_x^{(t,r)} cos(\frac{\theta}{2}) + I_x^{(t,s)} sin(\frac{\theta}{2}) \\ and \quad &e^{-i\theta I_x^{(r,s)}} I_y^{(t,r)} e^{i\theta I_x^{(r,s)}} = I_y^{(t,r)} cos(\frac{\theta}{2}) + I_x^{(t,s)} sin(\frac{\theta}{2}). \end{aligned} \tag{11}$$

The first commutator in eqn.(10), implies that, the coherence $I_x^{(t,r)}$ is rotated towards $I_x^{(t,s)}$, when the pulse is applied on transition (r,s), about y-axis. Whereas the second commutator in eqn.(10), implies that, $I_y^{(t,r)}$ is rotated towards $I_x^{(t,s)}$, under the r.f pulse, applied on transition (r,s) about the x-axis. Unlike in eqn.(8), the factor (1/2) in eqn.(10), indicates that, the angle of rotation is halved, when the transformed operator and the rotation operator have only one index in common. Furthermore the commutation relations of eqn.(10) are not cyclic. The commutation rules, given in eqn.(10), can also be visualized in three dimensional subspaces spanned by three orthogonal operators each, as shown in fig.2, for the subspaces (1,2) and (3,4), when the pulse is applied on (2,3) subspace. It may be noted that, in certain rotations the single quantum magnetization will evolve into a double or zero quantum coherence.

We now apply two consecutive selective π pulses on coherence $I_x^{(2,3)}$ (or state $|\psi_{23}\rangle$, eqn(3) and fig.(1b)), with phases respectively given by, y and $(y+\pi+\phi)$ in the xy plane. The evolution of the coherences $I_x^{(2,3)}$, $I_x^{(1,2)}$ and $I_x^{(3,4)}$ can be calculated by using the commutation relations given in eqn.s (8) and (10) (fig.2),

$$\begin{aligned}
&I_x^{(2,3)} \xrightarrow{I_y^{(2,3)}(\pi)} -I_x^{(2,3)} \xrightarrow{I_{(y+\pi+\phi)}^{(2,3)}(\pi)} cos(2\phi)I_x^{(2,3)} - sin(2\phi)I_y^{(2,3)},\\
&I_x^{(1,2)} \xrightarrow{I_y^{(2,3)}(\pi)} I_x^{(1,3)} \xrightarrow{I_{(y+\pi+\phi)}^{(2,3)}(\pi)} cos\phi I_x^{(1,2)} + sin\phi I_y^{(1,2)},\\
&I_x^{(3,4)} \xrightarrow{I_y^{(2,3)}(\pi)} -I_x^{(2,4)} \xrightarrow{I_{(y+\pi+\phi)}^{(2,3)}(\pi)} cos\phi I_x^{(3,4)} + sin\phi I_y^{(3,4)}.
\end{aligned} \tag{12}$$

The unitary operator associated with above operation (eqn.12) is identical to the phase shift gate U(2,3) of eqn.5, with $\Omega/2 = \phi$. In other words, the transformed coherences of equation (12), are identical to $(\sigma'_{rs} - (1/2)I^{(r,s)})$ of eqn.7, with $\phi = \Omega/2$. Hence one can conclude that, two selective π pulses, having phases y and $(y+\pi+\phi)$ respectively, applied on coherence $I_{(x)}^{(2,3)}$, evolves the state $|\psi_{23}\rangle$, over a closed loop on the Bloch sphere, and the solid angle subtended by the closed loop, at the center of the sphere is $\Omega = 2\phi$. However, in case of a π-phase shifted gate ($\phi = \pi$), the two π pulses, $(\pi)_y$ and $(\pi)_{(y+\pi+\pi=y)}$, shown in fig.(1b), can be combined in to a single $(2\pi)_y$ pulse. Such pulses are used in sections III, IV and V.

It is to be noted that, if the coherence of the (2,3) subspace is $I_{(\theta'+x)}^{(2,3)}$ in the xy plane, then the phases of π pulses will be $(y+\theta')$ and $(y+\theta'+\pi+\phi)$, and a π-phase shifted gate is achieved by applying $(2\pi)_{(y+\theta')}$ pulse. And if the (2,3) subspace is at equilibrium state, $I_z^{(2,3)}$, the phases of π pulses will be (θ'') and $(\theta''+\pi+\phi)$, where θ'' can be any axis in the xy plane, and a π-phase shifted gate is achieved by applying $(2\pi)_{\theta''}$ pulse.

From the above discussion it is concluded that, cyclic evolution of a two level subspace, by means of transition selective π pulses, acquires a geometric phase which also effects the other connected subspaces.

III. EXPERIMENTAL IMPLEMENTATION OF THE CONTROLLED PHASE SHIFT GATE

The system chosen is, dipolar coupled carbon and protons of the methyl group of $^{13}CH_3I$, partially oriented in ZLI-1132 liquid crystal. The three protons are, chemically and magnetically equivalent, and the total Hamiltonian is given by,

$$H = \omega_C I_z + 3\omega_H S_z + \sum_{i,j=1,2,3,\ i<j,} 2\pi[(J_{CH} I_z S_{zi} + 2D_{CH} I_z S_{z_i} + D_{HH}(3S_{z_i}S_{z_j} - S_i.S_j)], \tag{13}$$

where ω_H and ω_C are chemical shifts of protons and carbon respectively, D_{HH} is the residual dipolar coupling between identical protons (homonuclear coupling), and J_{CH} and D_{CH} are couplings of carbon (I) with protons (S). The scalar J coupling between identical protons does not effect the spectra in this case [39].

The energy level diagram (fig.3) of this system consists of 16 energy levels, eight of which belong to a symmetric manifold, and the other eight to two asymmetric manifolds [30]. The eight energy levels of the symmetric manifold can be considered as a 3-qubit system. In this system recently pair of pseudo pure states (POPS) and quantum gates (other than controlled phase shift gates) have been implemented by applying transition selective pulses [30, 31]. In this work we implement controlled phase shift gates by using non-adiabatic geometric phases obtained by using transition selective pulses.

The equilibrium ^1H and ^{13}C spectra are given in fig.(4a) and fig.(4b) respectively, wherein the various transitions are labeled in accordance with the notation used in fig.3. Since several transitions of symmetric and asymmetric manifolds, are degenerate, selection of symmetric states (SOSS) is performed to select the magnetization of the symmetric manifold [31]. However, since in the present experiments only the proton transitions are observed, we perform only a partial SOSS, in which the proton magnetization of symmetric manifold, is selectively retained, as explained below.

The entire experiment consists of 4 steps (as shown in fig.5).

(i) Selection of symmetric states (SOSS): The proton magnetization from asymmetric manifolds is saturated by using the pulse sequence $(\pi)^{h_3,h_4}$-G_z-$(\pi)^{h_3,h_4}$ (fig.5) , where $(\pi)^{h_3,h_4}$ represents two selective π pulses on h_3 and h_4 transitions, and G_z is the pulsed field gradient [31]. The π pulse on transitions h_3 and h_4 acts as a $\pi/2$ pulse on h_3' and h_4' [32], and a gradient dephases the coherences h_3' and h_4'. The second π pulse brings back the magnetization of symmetric manifold to its equilibrium value. Proton spectrum obtained by a small angle pulse followed by SOSS (fig.4c), has the intensities in the expected ratio 3:3:4:4:3:3, confirms the retention of proton magnetization only from the symmetric manifold.

(ii) An on resonance $(\pi/2)_y$ pulse is applied on the proton channel, which creates the proton coherences, h_1, h_2,

h_3, h_4, h_5 and h_6 . These coherences does not evolve under the chemical shift, since pulse is applied at resonance.

(iii) Controlled phase shift gates: As described in the previous section, cyclic evolution of a two level subspace by means of transition selective π pulses, acquire a geometric phase. In order to get only the geometric phase, one has to refocus the dynamical phase acquired due to internal Hamiltonian evolution. Spin echo sequence ($\tau - \pi - \tau$) is applied on protons (fig.5) to refocus hetero nuclear (^{13}C-^{1}H) coupling (dipolar and J). The geometric phase gates are obtained by applying two selective π pulses on carbon transitions, (fig.5), and the duration of the pulses is chosen such that the evolution of proton coherences under the homonuclear coupling makes a complete rotation (in multiple of 2π).

(iv) Detection: The phases of proton coherences $h_1 ... h_6$ (figures 6 and 7), are only due to cyclic geometric evolution of subspaces, confirming the implementation of phase shift gates, as explained below.

In fig.(6), geometric phases are obtained in (1,2) subspace , by applying two consecutive phase shifted selective π pulses on transition C_1. The phase of the first pulse is y, and that of second pulse is $(y + \pi + \phi)$, where ϕ=$\pi/2$, π, $3\pi/2$ and 2π, for fig.s 6(a), 6(b), 6(c), and 6(d) respectively. The unitary operator obtained by the above operation is, U(1,2)=diag[$e^{i\phi}$,$e^{-i\phi}$,1,1,1,1,1,1]. As expected, only the proton coherences h_1 and h_2 are effected by the unitary operator U(1,2), whereas the other proton coherences remain un affected. For example in fig(6a), the coherences $I_x^{(1,3)}(h_1)$ and $I_x^{(2,4)}(h_2)$, are transformed to $I_y^{(1,3)}$ and $-I_y^{(2,4)}$ giving dispersive signals of opposite sign, confirming the unitary operator U(1.2), for $\phi = \pi/2$.

Figure(7) shows the implementation of (π)-phase shift gates on two unconnected subspaces; U[(3,4),(5,6)]=diag[1,1,-1,-1,-1,-1,1,1], U[[(1,2),(3,4)]]=diag[-1,-1,-1,-1,1,1,1,1] and U[(1,2),(5,6)]=diag[-1,-1,1,1,-1,-1,1,1] (fig.s 7a, 7b and 7c respectively). Each of these gates require two $(2\pi)_y$ pulses on unconnected subspaces. U[(3,4),(5,6)] is implemented by applying $(2\pi)_y$ pulses on transitions C_2 and C_3, U[(1,2),(3,4)] is implemented by applying $(2\pi)_y$ pulses on transitions C_1 and C_2. Whereas U[(1,2),(5,6)] is implemented by applying $(2\pi)_y$ pulses on transitions C_1 and C_3. The signs of various transitions in the observed spectra of fig. 7, confirm the implementation of these phase shift gates. For example, the U[(3,4),(5,6)] gate inverts only the coherences h_1, h_2, h_5 and h_6.

IV. IMPLEMENTATION OF DEUTSCH-JOZSA (DJ) ALGORITHM

DJ algorithm determines in a single query, whether a given function is constant or balanced [13, 44]. A function is "constant" if it gives the same output for all inputs, and "balanced" if it gives one output for half the number of inputs and another for the remaining half. Classically for an n bit binary function, at least $(2^{n-1} + 1)$ queries are needed to determine whether the function is constant or balanced, whereas the DJ algorithm requires only a single query. The Cleve version [44] of the DJ algorithm requires an extra qubit (ancilla qubit) and uses controlled-not gates, whereas Collins version does not require the ancilla qubit but needs controlled phase shift gates [45]. While the Cleve version of DJ algorithm has been implemented both in weakly and strongly coupled systems [33, 46], the Collins version has been implemented only in weakly coupled systems [43]. Here we implement the Collins version of the DJ algorithm on a strongly coupled two qubit system, formed by dipolar coupled methyl protons of CH_3CN, oriented in ZLI-1132 liquid crystal. For a two qubit system there are 2 constant and 6 balanced functions, table(1). The quantum circuit of the Collins version of the DJ algorithm is shown in fig.8. The algorithm (fig.8) starts with a pure state (pseudo pure state in NMR) $|00\rangle$ which is converted to a equal superposition state of the basis states $|00\rangle$, $|01\rangle$, $|10\rangle$, and $|11\rangle$, by applying a pseudo Hadamard gate on both the qubits. Thereafter a unitary operator U_{f_i} (controlled phase shift gate) is applied, followed by detection. Theoretically, after U_{f_i} one has to apply the Hadamard gate. In NMR, a Hadamard gate is replaced by a pseudo Hadamard gate, which is implemented by a $(\pi/2)_y$ pulse, and for detection another $(\pi/2)_{-y}$ pulse is needed. These two pulses cancel each other and the result of the algorithm is available immediately after U_{f_i}. The Unitary operator U_{f_i} can be written as,

$$U_{fi} = \begin{pmatrix} (-1)^{f_i(00)} & 0 & 0 & 0 \\ 0 & (-1)^{f_i(01)} & 0 & 0 \\ 0 & 0 & (-1)^{f_i(10)} & 0 \\ 0 & 0 & 0 & (-1)^{f_i(11)} \end{pmatrix}, \tag{14}$$

where i=1 and 2 represent the "constant" function and i=3,4,5,6,7 and 8 represents the "balanced" functions, table 1.

The unitary operators, U_{f_1}, U_{f_3}, U_{f_5} and U_{f_7} are identical, up to an overall phase factor, of $e^{i\pi}$, to U_{f_2}, U_{f_4}, U_{f_6} and U_{f_8} respectively. Hence we implement only the unitary operators U_{f_1}, U_{f_3}, U_{f_5} and U_{f_7}.

The schematic energy level diagram of the dipolar coupled methyl protons of CH_3CN (without C-13 labeling) oriented in ZLI-1132 liquid crystal, is given in (fig.9). Transitions 1, 2 and 3 of symmetric manifold gives rise to three single quantum transitions at frequencies $\omega_o - 3D$, ω_o and $\omega_o + 3D$, with the intensity ratio 3:4:3, where D is the partially averaged (residual) dipolar coupling between the protons of CH_3CN and ω_o is their Larmor frequency. Transitions of asymmetric manifold also have the frequency ω_o identical to transition 2. The resultant spectrum is a 1:2:1 triplet as shown in fig.10a. The symmetric manifold of this system, consisting of four energy levels, can be treated as a two qubit system, and the labeling is given in fig.9.

The total experiment consists of 4 steps (as shown in fig. 11).

(i)Selection of symmetric manifold: The magnetization of asymmetric manifolds which contribute to central transition, is saturated by applying a π pulse on transitions 2, which acts as a $\pi/2$ pulse on transitions 4 and 5, a gradient pulse dephases the coherences, and the magnetization of the symmetric manifold is retained to its equilibrium value, with another π pulse. The relative integrated intensities of fig.10b (in the ratio 3:4:3) confirm the selection of symmetric manifold.

(ii)Creation of pseudo pure state (PPS) $|00\rangle$ [31]: The pseudo pure state $|00\rangle$ is prepared by applying a π pulse on transition 3 (fig. 11) , followed by a $\pi/2$ pulse on transition 2, a gradient pulse is applied to daphase the coherences. The proton spectrum of fig.10c, confirm the creation of the $|00\rangle$ PPS.

(iii) Superposition state followed by U_{f_i}: After the creation of $|00\rangle$ PPS, a pseudo Hadamard gate ($(\pi/2)_y$ on resonance pulse) creates a superposition of 4 basis states, and due to on-resonance pulse the coherences do not evolve under the chemical shift. It may be noted that unlike in weakly coupled spins, the state created here is not in uniform superposition of eigenstates, since the coefficients of various eigenstates are different [31]. However, as is shown here, the created coherent superposition can be utilized for quantum parallelism, to distinguish different classes of functions. The state of the system after a $(\pi/2)_y$ pulse is $|\psi\rangle = (1/2\sqrt{2})(|00\rangle + \sqrt{3}|01\rangle + \sqrt{3}|10\rangle + |11\rangle)$.

The unitary operator U_{f_i} of eqn.(14), is implemented by using non-adiabatic geometric phases, obtained by transition selective $(2\pi)_y$ pulses. The duration of transition selective pulses (fig. 11) is set such that the evolution due to homonuclear $^1H -^1 H$ dipolar coupling, makes a complete 2π rotation. U_{f_1} is a unit matrix which require no pulses. U_{f_3} and U_{f_5} are implemented by applying a single transition selective $(2\pi)_y$ pulse on transitions 2 and 3 respectively. U_{f_7} is implemented by applying two transition selective $(2\pi)_y$ pulses on transitions 2 and 3. The final state $|\psi_{f_i}\rangle$ (=$U_{f_i}|\psi\rangle$) can be written as,

$$\begin{aligned}
|\psi_{f_1}\rangle &= \frac{1}{2\sqrt{2}}(|00\rangle + \sqrt{3}|01\rangle + \sqrt{3}|10\rangle + |11\rangle),\\
|\psi_{f_3}\rangle &= \frac{1}{2\sqrt{2}}(|00\rangle - \sqrt{3}|01\rangle - \sqrt{3}|10\rangle + |11\rangle),\\
|\psi_{f_5}\rangle &= \frac{1}{2\sqrt{2}}(|00\rangle + \sqrt{3}|01\rangle - \sqrt{3}|10\rangle - |11\rangle),\\
|\psi_{f_7}\rangle &= \frac{1}{2\sqrt{2}}(|00\rangle - \sqrt{3}|01\rangle + \sqrt{3}|10\rangle - |11\rangle).
\end{aligned} \tag{15}$$

(iv) Detection: The phases of coherences 1, 2 and 3 confirm the final states $|\psi_{f_i}\rangle$. For constant function ($|\psi_{f_1}\rangle$), none of the peaks are inverted (fig.12a), whereas for the balanced functions ($|\psi_{f_3}\rangle$, $|\psi_{f_5}\rangle$ and $|\psi_{f_7}\rangle$), atleast one of the peaks is inverted (fig.12b,12c,12d respectively). The spectra of figure 12, confirm the implementation of Collins version of two-qbit DJ algorithm in the dipolar coupled spins by using non-adiabatic geometric phase gates.

V. IMPLEMENTATION OF PARITY ALGORITHM

The parity of a binary string X=$\{x_1, - - - -, x_N\}$, where x_i is 0 or 1, is even (odd) if x consists of even number (odd number) of 1's. The parity of X can be written as a Boolean function P(X)=$x_1 \oplus ..... \oplus x_N$. A classical computer has to call the oracle with each of the N possible inputs to determine P(X). Beals et. al and Farhi et. al showed that in a quantum computer the minimum number of oracle calls is N/2 [47, 48]. The parity algorithm has been implemented by Suter et.al [49] on a weakly coupled two qubit system. They have also shown that in case of ensemble quantum computers the complexity is further reduced [49]. In the quantum version, the parity of the binary string X is encoded in the Black box (oracle), such that the black box consists of N boolean variables, X=$\{x_1, ----, x_N\}$. The task is to determine the parity of the binary string, that is encoded in the oracle.

Recently it has been demonstrated that qutrits can be useful for certain purposes of quantum simulation, quantum computations and quantum communication, a qutrit has three states $|0\rangle$, $|1\rangle$ and $|2\rangle$ [50, 51, 52, 53, 54, 55]. In this work, we use a quantum circuit similar to the one used in ref.[49] and implement a qubit-qutrit parity algorithm in a single iteration of the oracle, starting with a mixed state. Non-adiabatic geometric phase gates are used to implement the required oracles. The qubit-qutrit system used here is obtained by orienting flouro-acetonitrile in ZLI-1132 liquid crystal. The two identical protons have one asymmetric and three symmetric eigen states (labeled as 0, 1, 2 in fig.14). The symmetric manifold of protons can be treated as a qutrit and the flourine nucleus as a qubit, yielding a 6 energy level system shown in fig.(14).

In the quantum circuit of the algorithm, the first register (fig.13) is assigned to flourine (qubit) and the second to protons (qutrit). The algorithm starts with a mixed state (ensemble of 6 basis states of a qubit-qutrit system), a pseudo Hadamard gate on the qubit register, creates single quantum coherences, whose phases are modulated by the oracle. Detection is done on the qubit register, which measures the single quantum coherences. After the pseudo Hadamard gate, the polarization of the qubit register consists the sum of three single quantum coherences, which can be written as,

$$I_x^{qubit} = |0\rangle\langle 1||0\rangle\langle 0| + |0\rangle\langle 1||1\rangle\langle 1| + |0\rangle\langle 1||2\rangle\langle 2|, \tag{16}$$

where the first part of each term indicates the single quantum coherence of the qubit and second part indicates the state of qutrit.

The oracle in (fig.13) is defined as

$$O = \begin{pmatrix} (-1)^{x_1} & 0 & 0 & 0 & 0 & 0 \\ 0 & (-1)^{x_2} & 0 & 0 & 0 & 0 \\ 0 & 0 & (-1)^{x_3} & 0 & 0 & 0 \\ 0 & 0 & 0 & (-1)^{x_4} & 0 & 0 \\ 0 & 0 & 0 & 0 & (-1)^{x_5} & 0 \\ 0 & 0 & 0 & 0 & 0 & (-1)^{x_6} \end{pmatrix}, \tag{17}$$

Table(2) shows the unitary operators of the oracle corresponding to different strings, X=$\{x_1, ..., x_6\}$, of various parities. Here, one should note that the oracles, for parities 0, 1 and 2 are identical to that of parities 6, 5 and 4 respectively, up to an overall phase factor $e^{i\pi}(= -1)$. Hence we implement only the oracles of parities 0, 1, 2 and 3. For even parity, even number of terms of eqn.(16) acquire a phase factor $e^{i\pi}$, and for odd parity odd number of terms acquire a phase factor $e^{i\pi}$. Hence, by measuring single quantum coherences, one can determine the parity that is encoded to the 6 digit binary string.

The equilibrium spectra of ^1H and ^{19}F are shown in fig.15a and 15b respectively. In the flourine spectrum, the intensity of central transition is twice that of satellite transitions, due to the overlap of the transition of the asymmetric manifold.

The experiment consists of 3 steps (as shown in fig.16)

(i) Selection of symmetric manifold (SOSS): The magnetization from asymmetric manifold is saturated by using the pulse sequence (fig.16), known as SOSS. A gradient pulse following a $\pi/2$ pulse on flourine, saturates the flourine magnetization. The flourine magnetization of symmetric manifold is retrieved by partial polarization transfer from ^1H to ^{19}F by applying selective π pulses on H_2 and H_3 transitions followed by a selective $3\pi/4$ pulse on F_2 transition. A final gradient pulse dephases the transverse magnetization created during the process. The spectrum obtained by a small angle pulse after SOSS, gives the relative intensities in the expected ratio 1:1:1 (fig.15c), confirming SOSS. The six energy levels of the symmetric manifold can be treated as a 6 digit binary string X=$\{x_1, ..., x_6\}$.

(ii) Implementation of pseudo Hadamard gate followed by oracle: A $(\pi/2)_y$ on resonance pulse, applied on ^{19}F, implements a pseudo Hadamard gate, and the created coherences does not evolve under the chemical shift, since the pulse is applied at resonance. The unitary operators of the oracle, are implemented by using non-adiabatic geometric phases. The phase shift gates $d^{\phi}_{H_i}$ or $d^{\phi}_{F_i}$ (Table 3) can be implemented by applying two transition selective π pulses respectively on transitions H_i or F_i with phases y and $(y + \pi + \phi)$, and the duration of the pulses is set such that the evolution under the hetero nuclear couplings $(J + 2D)$ makes a complete 2π rotation. However spin echo sequence $(\tau - \pi - \tau)$ is also used which refocuses hetero nuclear couplings and chemical shift evolution (if any). Since the unitary operators of the oracle are diagonal matrices, one can sandwich different phase shift gates to get a desired phase shift gate, as shown in Table(2), up to an overall phase factor. For example O_1^4 is a product of $d_{H_2}^{\pi/3}$, $d_{H_3}^{\pi/6}$, $d_{H_4}^{-\pi/2}$, $d_{F_1}^{\pi/6}$, $d_{F_3}^{\pi/3}$ (up to an overall phase factor $e^{i\pi/6}$), which is implemented by three pairs of selective π pulses on ^1H channel and two pairs of π pulses on ^{19}F channel, fig.16. Similarly one can implement remaining oracles by sandwiching various phase shift gates, as shown in Table 2.

(iii) Detection: Single quantum coherences of flourine are measured. Depending on the number of peaks that are inverted the parity is determined such that, for even parity, even number (0 or 2) of peaks are inverted, while for odd parity, odd number (1 or 3) of peaks are inverted. The figures 17(a), 17(b), 17(c) and 17(d) indicate the odd parity, which are obtained by implementing O_1^2, O_1^4, O_1^6 and $O_3^{(2,4,6)}$ (Table 2) respectively. Figures 17(e), 17(f), 17(g) and 17(h) indicate the even parity, which are obtained by implementing I, $O_2^{(4,6)}$, $O_2^{(2,6)}$ and $O_2^{(2,4)}$ (Table 2) respectively. These spectra clearly confirm the implementation of the parity algorithm in this qubit-qutrit system, utilizing non-adiabatic geometric phase gates.

VI. CONCLUSIONS

Conventionally, controlled phase shift gates which are basic elements in many quantum circuits, are implemented by the combination of qubit selective pulses and evolution under the weakly coupled Hamiltonian. In order to achieve higher number of qubits in NMR, one explores dipolar couplings which are larger in magnitude, yielding strongly coupled spectra. In such systems since the Hamiltonian consists of non-secular terms it is difficult to apply qubit selective pulses. The present method to implement controlled phase shift gates, does not require qubit selective pulses and evolution under Hamiltonian. While in this paper, we have used the systems containing only one homo nuclear dipolar coupling, the method is being extended to systems containing more than one homo nuclear dipolar coupling, by using suitable refocusing schemes and by using strongly modulated pulses [56]. This method can also be applied to quadrapolar systems. This method thus contributes towards the use of strongly coupled spins for NMR Quantum computing.

ACKNOWLEDGMENTS

Useful discussions with Dr. Ranabir Das and H. S. Vinay Deepak are gratefully acknowledged. The use of AV-500 NMR spectrometer funded by the department of science and Technology (DST), New Delhi, at the NMR research center (former Sophisticated Instruments Facility), Indian Institute of Science, Bangalore, is gratefully acknowledged. A.K. acknowledges DAE for Raja Ramana Fellowship, and DST for a research grant on "Quantum Computing using NMR techniques".

Table 1. Constant and Balanced functions for a two qubit system

	Constant		Balanced					
x	$f_1(x)$	$f_2(x)$	$f_3(x)$	$f_4(x)$	$f_5(x)$	$f_6(x)$	$f_7(x)$	$f_8(x)$
00	0	1	0	1	0	1	0	1
01	0	1	1	0	0	1	1	0
10	0	1	1	0	1	0	0	1
11	0	1	0	1	1	0	1	0

Table 2. Unitary operators of the oracle, for various parities of a binary string X

Parity	X	O (oracle)
0	$\{0,0,0,0,0,0\}$	diag[1,1,1,1,1,1]=I
1	$\{0,1,0,0,0,0\}$	$O_1^2 = diag[1,-1,1,1,1,1] = d_{H_2}^{-2\pi/3}.d_{H_3}^{\pi/6}.d_{H_4}^{-\pi/2}.d_{F_1}^{\pi/6}.d_{F_3}^{\pi/3}$
1	$\{0,0,0,1,0,0\}$	$O_1^4 = diag[1,1,1,-1,1,1] = d_{H_2}^{\pi/3}.d_{H_3}^{\pi/6}.d_{H_4}^{-\pi/2}.d_{F_1}^{\pi/6}.d_{F_3}^{\pi/3}$
1	$\{0,0,0,0,0,1\}$	$O_1^6 = diag[1,1,1,1,1,-1] = d_{H_2}^{\pi/3}.d_{H_3}^{\pi/6}.d_{H_4}^{\pi/2}.d_{F_1}^{\pi/6}.d_{F_3}^{\pi/3}$
2	$\{0,0,0,1,0,1\}$	$O_2^{(4,6)} = diag[1,1,1,-1,1,-1] = d_{H_4}^{\pi}$
2	$\{0,1,0,0,0,1\}$	$O_2^{(2,6)} = diag[1,-1,1,1,1,-1] = d_{H_2}^{\pi}.d_{H_4}^{\pi}$
2	$\{0,1,0,1,0,0\}$	$O_2^{(2,4)} = diag[1,-1,1,-1,1,1] = d_{H_2}^{\pi}$
3	$\{0,1,0,1,0,1\}$	$O_3^{(2,4,6)} = diag[1,-1,1,-1,1,-1] = d_{H_3}^{\pi/2}.d_{H_4}^{-\pi/2}.d_{F_1}^{\pi/2}.d_{F_3}^{\pi}$

Table 3. Unitary operators of controlled-ϕ phase shifted gates

$d_{H_i(F_i)}^{\theta}$
$d_{F_1}^{\phi} = diag[e^{i\phi}, e^{-i\phi}, 1, 1, 1, 1]$
$d_{F_2}^{\phi} = diag[1, 1, e^{i\phi}, e^{-i\phi}, 1, 1]$
$d_{F_3}^{\phi} = diag[1, 1, 1, 1, e^{i\phi}, e^{-i\phi}]$
$d_{H_1}^{\phi} = diag[e^{i\phi}, 1, e^{-i\phi}, 1, 1, 1]$
$d_{H_2}^{\phi} = diag[1, e^{i\phi}, 1, e^{-i\phi}, 1, 1]$
$d_{H_3}^{\phi} = diag[1, 1, e^{i\phi}, 1, e^{-i\phi}, 1]$
$d_{H_4}^{\phi} = diag[1, 1, 1, e^{i\phi}, 1, e^{-i\phi}]$

[1] P. Benioff, Phys. Rev. Lett. **48**, 1581 (1982).

[2] D. Deutsch, Proc. R. Soc. London, Ser. A 400, 97 (1985).

[3] R. Feynman, *Int. j. Theor. phys.* **21**, 467 (1982).

[4] C.H. Bennett, Int. J. Theor. Phys. 21 905 (1982).

[5] S. Lloyd, Science 261, 1569 (1993).

[6] Barenco A., Deutsch D., Ekert A., and Jozsa R., Phys. Rev. Lett. **74**, 4083 (1995).

[7] I. L. chuang, L. M. K. Vanderspyen, X. Zhou, D. W. Leung, and S. Llyod, *Nature (london)*, **393**, 1443 (1998).

[8] J.A. Jones and M. Mosca, *J. Chem. Phys.* **109**, 1648 (1998).

[9] I.L. Chuang, N. Gershenfeld, M. Kubinec, Phys. Rev. Lett. **80**, 3408 (1998).

[10] T. S. Mahesh, Kavita Dorai, Arvind, Anil Kumar, *J. Mag. Res.* **148**, 95 (2001).

[11] J. A. Jones, Fort Der physik 48 909 (2000).

[12] P. W. Shor, *SIAM Rev.* **41**, 303-332 (1999).

[13] D. Deutsch and R. Jozsa, *Proc. R. Soc. Lond. A* **439**, 553 (1992).

[14] L.K. Grover, *Phys. Rev. Lett.* **79**, 325 (1997).

[15] J. Gruska "Quantum Computing", Mcgraw-Hill, London UK, 1999.

[16] D. Bouwnmeester, A. Ekert, A. Zeilinger(Eds.), "The Physics of Quantum Information", Springer, Berlin, 2000.

[17] M.A. Nielsen , I.L. Chuang, "Quantum Computation and Quantum Information". Cambridge University Press, Cambridge, U.K. 2000.

[18] J. A. Jones, V. Vedral, A.Ekert and G. Castagnoli, Nature **403**, 869 (2000).

[19] M. V. Berry, Proc. Roy. Soc. London A **392**, 45 (1984), and Nature (London) **326**, 277 (1987).

[20] Phys. Rev. Lett. **51**, 2167 (1983).

[21] D. Suter, G. Chingas, R. A. Harris and A. Pines, Mol. Phys. **61**, 1327 (1987).

[22] J.A. Jones, V. Vedral, A. Ekert and G. Castagnoli, Nature **403**, 869 (2000).

[23] A. Ekert, M. Ericsson, P. Hayden, H. Inamori, J.A. Jones, D. K. L. Oi, V. Vedral, Journal of modern optics **47**, 2501 (2000).

[24] S. L. Zhu and Z. D. Wang, Phys. Rev. Lett. **89**, 097902 (2002); *Phys. Rev. A* **66**, 042322 (2002).

[25] X. B. Wang and M. Keiji, Phys. Rev. Lett. **87**, 097901 (2001).

[26] Y. Aharnov and J. Anandhan, Phys. Rev. Lett. **58**, 1593 (1987).

[27] D. Suter, K. T. Mueller and A. Pines, Phys.Rev.Lett. **60**, 1218 (1988).

[28] Ranabir Das and Anil Kumar, *J. Magn. Reson.* **177**, 318 (2005).

[29] J.A. Jones, M. Mosca, and R. H. Hansen, *Nature (London)* **393**, 344 (1998).

[30] B. M. Fung, Phys. Rev. A **63**, 022304 (2001).

[31] T. S. Mahesh, Neeraj Sinha, K. V. Ramanathan, and Anil Kumar *Phys. Rev. A* **65**, 022312 (2002).

[32] C. L. Mayne, J. M. Bernassau, and D. M. Grant, *J. Chem. Phys* **76**, 257 (1982).

[33] T. S. Mahesh, Neeraj Sinha, Arindam Ghosh, Ranabir Das, N.Suryaprakash, Malcom H.Levitt, K. V. Ramanathan, and Anil Kumar *Current Science* **85**, 932 (2003); xxx.lanl.gov/abs/quant-ph/0212123.

[34] Ranabir Das, P.hD. thesis, Indian Institute of Science, Bangalore (2004) and XXI^{st} Int. Conf. Magn. Res. Biol. Systems, January 2005, Hyderabad, India, P9.

[35] Jae-Seung Lee and A. K. Khitrin *J. Chem. Phys* **122**, 041101 (2005).

[36] M. Marjanska, I. L. Chuang, and M. G. Kubinec, J. Chem. Phys. **112**, 5095 (2000).

[37] C. S. Yanoni, M. H. Sherwood, D. C. Miller, I. L. Chuang, L. M. K. Vandersypen, and M. G. Kubinec, Appl. Phys. Lett. **75**, 3563 (1999).

[38] Ranabir Das and Anil Kumar, *J. Magn. Reson.* **170** 310 (2004).

[39] R. R. Ernst, G.Bodenhausen, And A. Wokaun, Principles of Nuclear Magnetic Resonance in One and Two Dimensions, Oxford University Press 1987.

[40] A. Wokaun and R. R. Ernst *J. Chem. Phys.* **67**,No.4 (1977).

[41] D.G. Cory, A. F. Fahmy, and T. F. Havel, Proc. Natl. Acad. sci. USA 94, 1634 (1997).

[42] N. Gershenfield and I. L. Chuang, Science 275, 350 (1997).

[43] Oliver Mangold, Andreas Heidebrecht, and Michael Mehring*Phys. Rev. A* **70**, 042307 (2004).

[44] R. Cleve, A. Ekert, C. Macchiavello, and M. Mosca, *Proc. R. Soc. Lond. A* **454**, 339 (1998).

[45] David Collins, K. W. Kim, and W. C. Holton *Phys. Rev. A* **58**, 1633 (1998).

[46] Kavita Dorai, Arvind, and Anil Kumar *Phys. Rev. A* **61**, 042306 (2000).

[47] R. Beals, H. Buhrman, R. Cleve, M. Mosca, and R. de Wolf, *J.ACM* **48**, 778 (2001).

[48] E. Farhi, J. Goldstone, S. Gutmann, and M. Sipser, *Phys. Rev. Lett.* **81**, 5442 (1998).

[49] Ralf Stadelhofer, Dieter Suter, and Wolfgang Banzhaf *Phys. Rev. A* **71**, 032345 (2005).

[50] B. M. Terhal, I. L. Chuang, D. P. Divincenzo, M. Grassl and J. A. Smolin, Phys. Rev. A **60**, 881-885 (1999).

[51] A. P. Flitney and D. Abbott, Phys. Rev. A **65**, 062318 (2002).

[52] M. Fitzi, N. Gisin and U. Maurer, Phys. Rev. Lett **87**, 217901 (2001).

[53] Ranabir Das, Avik Mitra, S. V. Kumar and Anil Kumar, International Journal of Quantum Information Processing **1**, 387 (2003).

[54] A. B. Klimov, R. Guzman, J. C. Retamal, and Saavedra, Phys. Rev. A **67**, 062313 (2003).

[55] Paul B. slater, Phys. Rev. A **71**, 052319 (2005).

[56] Evan M. Fortunato, Marco A. Pravia, Nicolas Boulani, Grum Teklemariam, Timothy F. Havel, David G. Cory, *J. Chem. Phys.* **116 (17)**, 7599-7606 (2002).

FIGURE CAPTIONS

(1). (a) Schematic energy level diagram of a four level system, such that the single quantum magnetization of the subspaces (1,2), (2,3) and (3,4) is directly observable. (b) Evolution of state $|\psi_{rs}\rangle$ (r,s=1,2 and 3, s=r+1), over a closed loop on the Bloch sphere, by applying two transition selective π pulses on transition (r,s) with phases y and $(y+\pi+\pi=y)$. Solid angle subtended by this closed loop at the center of the sphere is, 2π.

(2). Rotations in subspaces spanned by orthogonal operators, of the 4 level system of fig.(1a). (a), (b), (c) and (d) follow the commutation relations, respectively given by, $[I_x^{(1,2)}, I_x^{(1,3)}] = \frac{i}{2}I_y^{(2,3)}$, $[I_y^{(1,2)}, I_x^{(1,3)}] = \frac{i}{2}I_x^{(2,3)}$, $[I_x^{(2,4)}, I_y^{(3,4)}] = \frac{i}{2}I_x^{(2,3)}$ and $[I_x^{(2,4)}, I_x^{(3,4)}] = \frac{i}{2}I_y^{(2,3)}$ (eqn.10). Each of the commutation rules follow the transformation property given in eqn.(11), for example, for fig.(a) $[I_x^{(1,2)}, I_x^{(1,3)}] = \frac{i}{2}I_y^{(2,3)}$, means that a $(\phi)y$ pulse applied on transition (2,3), acts as a $\phi/2$ pulse on transition (1,2), hence $I_x^{(1,2)}$ is transformed to $(I_x^{(1,2)}cos(\phi/2) + I_x^{(1,3)}sin(\phi/2))$. (Adopted from ref.s [39], [40])

(3). The schematic energy level diagram of dipolar coupled protons and carbon of $^{13}CH_3I$, partially oriented in a liquid crystal. There are 16 energy levels, eight of which belong to a symmetric manifold and the other eight to two groups of asymmetric manifolds. h_i, h_i' and h_i'' represent proton transitions and C_i, C_i' and C_i'' represent carbon transitions. All transitions with identical subscript are degenerate, eg. C_i, C_i' and C_i'' have identical frequencies, as well as h_i, h_i' and h_i'', (see fig.4).

(4). Proton (a) and carbon (b) equilibrium spectra of oriented $^{13}CH_3I$ recorded at 500 MHz of proton frequency. The labeling of transitions are in accordance with the notation used in fig.3. The transitions h_2, h_4 and h_6 (and also h_1, h_3 and h_5) are split by homonuclear dipolar coupling, and the splitting is equal to $3D_{HH}$ which has a value 3553 Hz, fig. (4a). The C-H splitting is equal to $(2D_{CH} + J_{CH})$, which has a value 2053 Hz, fig. (4b). The relative experimental integrated intensities are in the ratio; for ^1H 0.98:1.00:2.00:2.02:1.00:0.99 (theoretical ratios are 1:1:2:2:1:1), and for ^{13}C 0.98:3.02:3.00:1.00 (theoretical ratios are 1:3:3:1). (c) ^1H spectrum, obtained using a small angle measuring pulse, after implementation of SOSS. The SOSS is implemented here by the pulse sequence $(\pi)^{h_3,h_4} - G_z - (\pi)^{h_3,h_4}$. The relative experimental integrated intensities are in the ratio 2.97:3.02:4.05:4.02:3.00:2.98 (theoretical ratios are 3:3:4:4:3:3).

(5). The pulse sequence for implementation of Geometric phase shift gate (GPSG) U(1,2)=diag[$e^{i\phi}$,$e^{-i\phi}$,1,1,1,1,1,1]. The pulse sequence consists of four parts; (i) SOSS:$[(\pi)^{h_3,h_4} - G_z - (\pi)^{h_3,h_4}]$, (ii) Pseudo Hadamard gate on protons: $(\pi/2)_y^{^1H}$, (iii) Geometric phase shift gate: $[\tau - \pi - \tau]$, $((\pi)_y^{C_1}\ (\pi)_{y+\pi+\phi}^{C_1})$ during second τ period, evolves the z magnetization of (1,2) subspace over a closed loop on the Bloch sphere, with solid angle 2ϕ (iv) Detection of proton resonances.

(6). Proton spectra obtained after the implementation of Geometric phase shift gate

U(1,2)=diag[$e^{i\phi}$,$e^{-i\phi}$,1,1,1,1,1,1] (pulse sequence of fig.5). (a) to (d) respectively, are for $\phi = \pi/2, \pi, 3\pi/2$ and 2π. Since the Hamiltonian evolution during transition selective pulses is refocused, the phases of the the peaks in the spectra are entirely due to geometric phases and confirm the implementation of geometric phase shift gates. The transition selective carbon pulses are low power Gaussian pulses of duration 5.65 msec (=$\tau/2$).

(7). Experimental proton spectra obtained after implementation of (π)-phase shifted gates on two unconnected subspaces. These gates are obtained by applying two transition selective $(2\pi)_y$ pulses on carbon transitions, during the second τ period in the pulse sequence of fig.5. The length of transition selective 2π pulse is identical as that of π pulse but has double the pulse power, such that the dynamic phase remains refocused. Spectra corresponding to geometric phase shift gates (a) U[(3,4),(5,6)]=diag[1,1,-1,-1,-1,-1,1,1] implemented by applying $(2\pi)_y$ pulses on transitions C_2 and C_3. In this experiment the coherences h_1, h_2, h_5 and h_6 acquire a Geometric phase of π while the coherences h_3 and h_4 acquire a phase of 2π. (b) U[(1,2),(3,4)]=diag[-1,-1,-1,-1,1,1,1,1] implemented by applying $(2\pi)_y$ pulses on transitions C_1 and C_2 yielding the proton spectrum with coherences h_3 and h_4 yielding a π phase shift. (c) U[(1,2),(5,6)]=diag[-1,-1,1,1,-1,-1,1,1], implemented by applying $(2\pi)_y$ pulses on transitions C_1 and C_3, yielding the proton spectrum, in which all proton coherences acquire π phase shift.

(8). Quantum circuit for implementation of two qubit Deutsch-Jozsa algorithm (Collins version). The pseudo Hadamard gate creates superposition of the four basis states. U_{fi} is the unitary transformation, given in eqn.14, corresponding to the function f_i given in table(I). The final Hadamard gate in the original circuit is canceled by a detection pulse (pseudo Hadamard gate). Hence the result of the algorithm is available immediately after U_{fi}.

(9). Schematic energy level diagram of dipolar coupled oriented CH_3CN. The four levels of symmetric manifold are labeled as, basis states of a two qubit system. Transitions 2, 4 and 5 are degenerate, as shown in fig. 10(a).

(10). (a) Equilibrium proton spectrum of oriented CH_3CN. The labeling of transitions are in accordance with the notations used in fig.(9). The relative integrated intensities are in the ratio 1.00:1.99:0.98 (theoretical ratios are 1:2:1), and the splitting $3D_{HH}$ has a value 4968 Hz. (b) spectrum obtained by a small angle pulse after SOSS by the pulse sequence $(\pi)^2 - G_z - (\pi)^2$ (fig.11). The relative experimental integrated intensities are in the ratio 3.02:3.98:2.97 (theoretically expected 3:4:3). (c) spectrum obtained by a small angle pulse after the preparation of pseudo pure state $|00\rangle$, by using the pulse sequence, $(\pi)^3 - (\pi/2)^2 - G_z$ (fig.11).

(11). The pulse sequence for the implementation of two qubit Deutsch-Jozsa algorithm (fig.8), consists of four parts; (i) SOSS: $(\pi)^2 - G_z - (\pi)^2$, (ii) Pseudo pure state $|00\rangle$: $(\pi)^3 - (\pi/2)^2 - G_z$, (iii) Coherent superposition followed by U_{f_7}=diag[1 -1 1 -1]: A $(\pi/2)_y$ on resonance pulse creates a superposition state $|\psi\rangle = (1/2\sqrt{2})(|00\rangle + \sqrt{3}|01\rangle + \sqrt{3}|10\rangle + |11\rangle)$, U_{f_7} is implemented by $[(2\pi)_y^2\ (2\pi)_y^3]$. The duration of transition selective pulses (5.229 msec) is such that the evolution due to dipolar coupling makes a complete 2π rotation and thus the phases are only due to cyclic geometric evolution of subspaces. (iv) Detection of single quantum coherences.

(12). Implementation of two qubit Deutsch-Jozsa algorithm on oriented CH_3CN, by using the pulse sequence shown in fig.11. Transition selective pulses are of Gaussian shape with duration 5.229 msec. After pseudo Hadamard gate (fig.11), controlled phase shift gate U_{f_i} is implemented. (a) U_{f_1} is identity matrix which require no pulse, hence single quantum coherences are measured immediately after pseudo Hadamard gate. The integrated intensities are in the ratio, 1.69:3.00:1.72 (theoretically expected $\sqrt{3}$:3:$\sqrt{3}$ [31]), confirms state $|\psi_{f1}\rangle$ of eqn.15. (b) U_{f_3} (c) U_{f_5}, are implemented by applying a single $(2\pi)_y$ pulse on transitions 2 and 3 respectively. (d) U_{f_7} is implemented by applying two $(2\pi)_y$ pulses on transitions 2 and 3. In fig.(a), none of the peaks are inverted, indicates the constant function. The fig.s(b,c and d) confirms the final states $|\psi_{f3}\rangle$, $|\psi_{f5}\rangle$ and $|\psi_{f7}\rangle$ of eqn.(15), and atleast one of the peaks are inverted, indicates the balanced functions.

(13). Quantum circuit for implementing qubit-qutrit parity algorithm. Initial state is a mixed state followed by a pseudo Hadamard gate (h) on qubit register. Unitary operators of oracle are controlled phase shift gates, given in table(2) for various parities. The final step is the measurement on qubit register, which in NMR is the direct signal acquisition of resulting single quantum coherences.

(14). Schematic energy level diagram of oriented CH_2FCN, consisting of symmetric and asymmetric manifolds. Flourine transitions are labeled as F_i and F'_i and that of protons as H_i. The transitions F_2 and F'_2 are degenerate (see fig.15b).

(15). (a) and (b) are, respectively, equilibrium proton and flourine spectra of oriented CH_2FCN. In the proton spectrum, experimental integrated intensities are in the ratio 0.98:1.00:0.99:0.98 (theoretical ratios are 1:1:1:1), and that of flourine are in the ratio 0.99:2.01:1.00 (theoretical ratios are 1:2:1). The transitions H_1 and H_3 (also H_2 and H_4) are split by homonuclear diploar coupling. The splitting is equal to $3D_{HH}$ which has a value 5694 Hz. The ^{19}F-^{1}H splitting in (b) is equal to $(2D_{FH}+J_{FH})$, which has a value 473 Hz. (c) Flourine spectrum obtained by a small angle pulse after SOSS by the pulse sequence $\pi/2 - G_z - (\pi)^{H_2,H_3} - (3\pi/4)^{F_2} - G_z$ (fig.16). The relative experimental integrated intensities are in the ratio 1.00:1.02:0.98 (theoretical ratios are 1:1:1).

(16). The pulse sequence to implement qubit-qutrit parity algorithm (fig.13). The pulse sequence consists of four parts; (i) SOSS: $\pi/2 - G_z - (\pi)^{H_2,H_3} - (3\pi/4)^{F_2} - G_z$, (ii) Pseudo Hadamard gate: On resonance $(\pi/2)_y^{^{19}F}$ pulse, (iii) Oracle O_1^4, shown in Table 2: During first τ period three pairs of transition selective proton π pulses $[(\pi)_y^{H_2}(\pi)_{(y+\pi+\pi/3)}^{H_2}]$ $[(\pi)_y^{H_3}(\pi)_{(y+\pi+\pi/6)}^{H_3}]$ $[(\pi)_y^{H_4}(\pi)_{(y+\pi-\pi/2)}^{H_4}]$ are applied, which respectively implement $d_{H_2}^{\pi/3}$, $d_{H_3}^{\pi/6}$ and $d_{H_4}^{-\pi/2}$, and during second τ period two pairs of transition selective flourine π pulses $[(\pi)_y^{F_1}(\pi)_{(y+\pi+\pi/6)}^{F_1}][(\pi)_y^{F_3}(\pi)_{(y+\pi+\pi/3)}^{F_3}]$ are applied, which respectively implement $d_{F_1}^{\pi/6}$ and $d_{F_3}^{\pi/3}$. The duration of transition selective π pulses is set such that the evolution under the hetero nuclear couplings $(J + 2D)$ makes a complete 2π rotation. (iv) Detection of single quantum coherences of flourine, from which the parity can be determined.

(17). Implementation of qubit-qutrit parity algorithm, by using the pulse sequence shown in fig.16. The transition selective π pulses, for both proton and flourine, are of Gaussian shape with duration 12.85 msec. For odd (even) parity odd (even) number of peaks are inverted, in other words odd (even) number of single quantum coherences of flourine acquire a phase π. (a), (b), (c) and (d) indicate the odd parity which are obtained by implementing O_1^2, O_1^4, O_1^6 and $O_3^{(2,4,6)}$ (Table 2) respectively. (e), (f), (g) and (h) indicate the even parity, which are obtained by implementing I, $O_2^{(4,6)}$, $O_2^{(2,6)}$ and $O_2^{(2,4)}$ (Table 2) respectively.

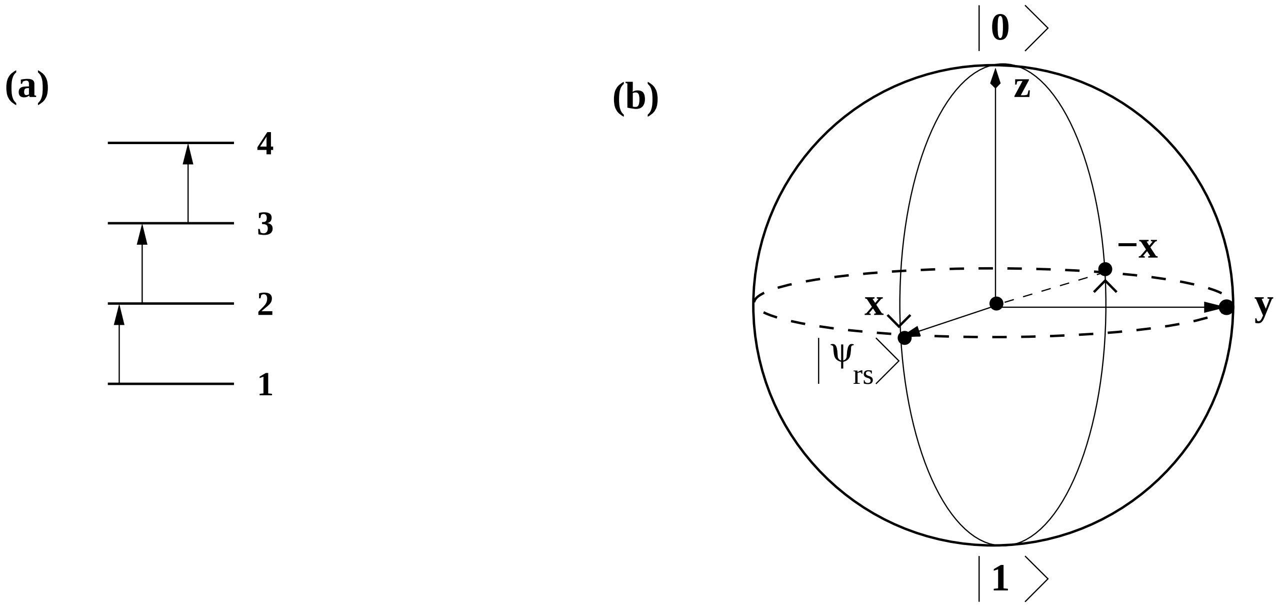

FIG. 1:

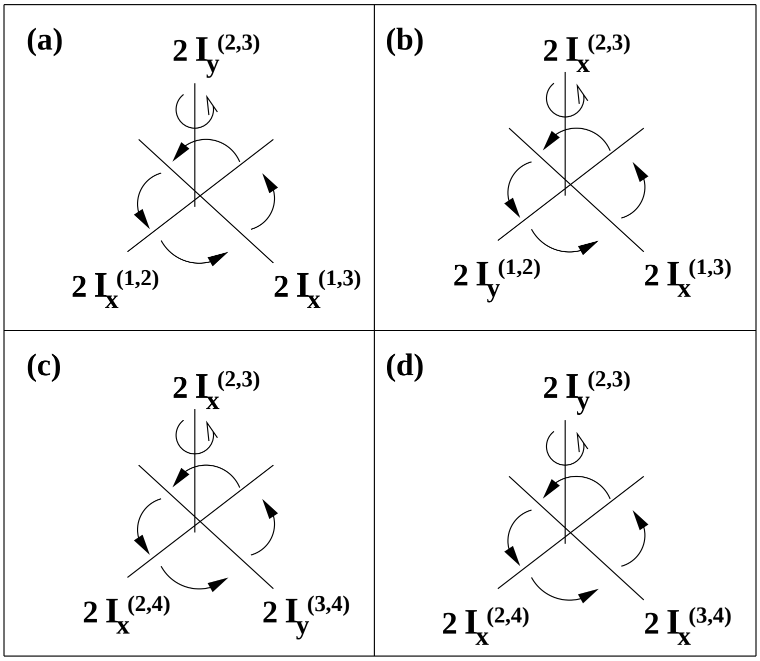
(a)
2 I_y^(2,3)
2 I_x^(1,2)
2 I_x^(1,3)
(b)
2 I_x^(2,3)
2 I_y^(1,2)
2 I_x^(1,3)
(c)
2 I_x^(2,3)
2 I_x^(2,4)
2 I_y^(3,4)
(d)
2 I_y^(2,3)
2 I_x^(2,4)
2 I_x^(3,4)

FIG. 2:

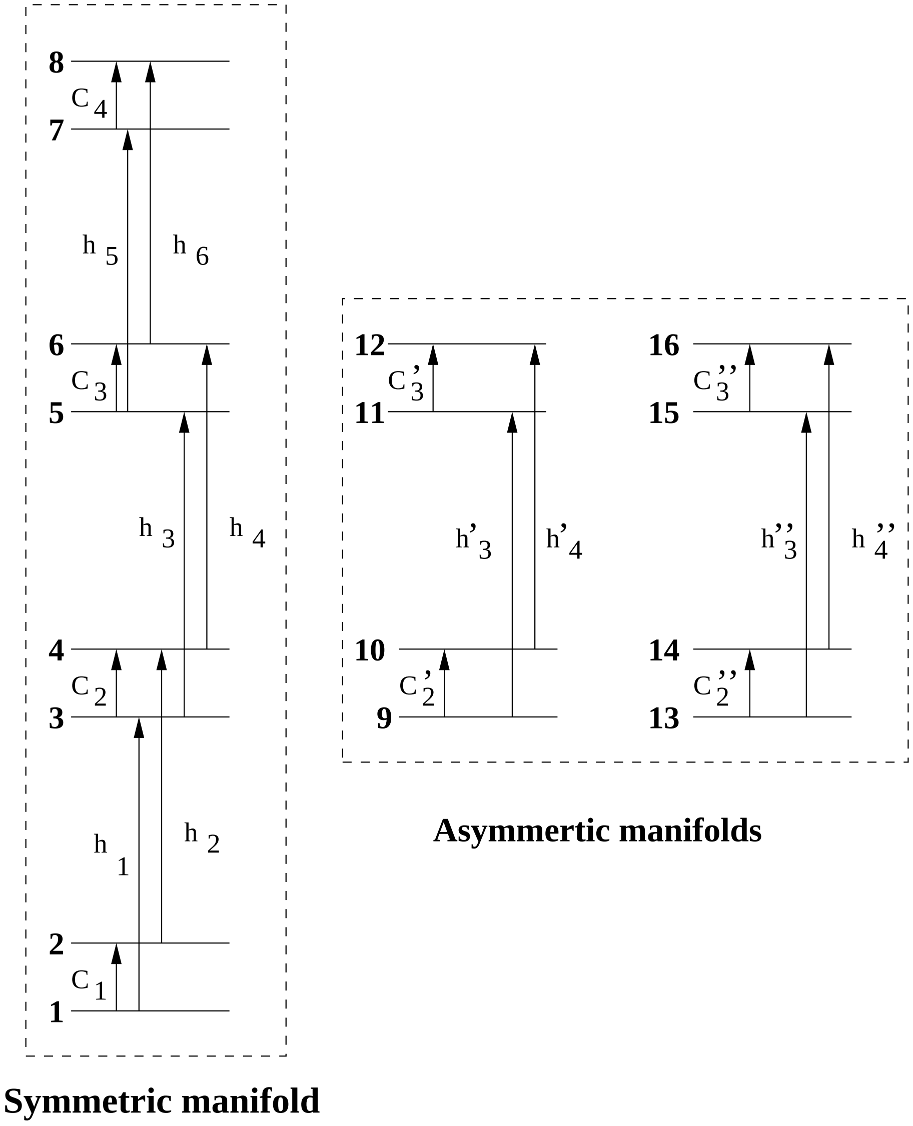
8
7
C 4
h 5
h 6
6
5
C 3
h 3
h 4
4
3
C 2
h 1
h 2
2
1
C 1
Symmetric manifold
12
11
C'3
h'3
h'4
10
9
C'2
16
15
C''3
h''3
h''4
14
13
C''2
Asymmertic manifolds

FIG. 3:

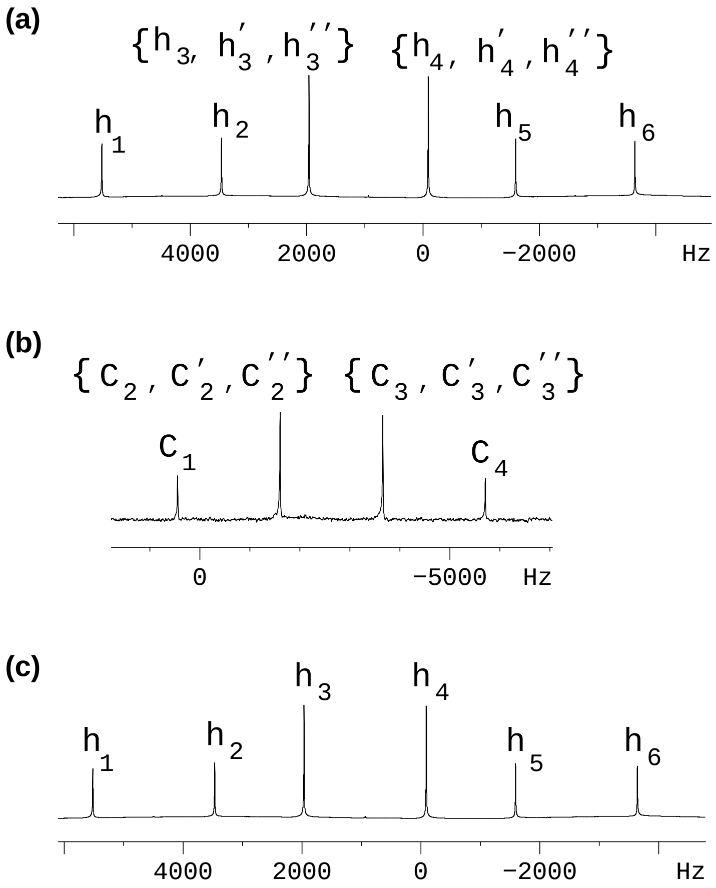
(a)
{h3, h'3, h''3} {h4, h'4, h''4}
h1
h2
h5
h6
4000
2000
0
−2000
Hz
(b)
{C2, C'2, C''2} {C3, C'3, C''3}
C1
C4
0
−5000
Hz
(c)
h3
h4
h1
h2
h5
h6
4000
2000
0
−2000
Hz

FIG. 4:

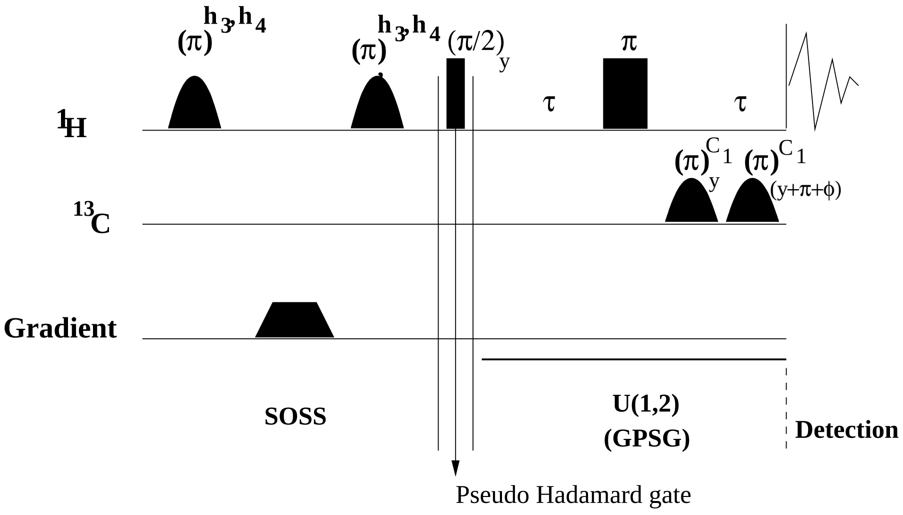
(π)h3,h4
(π)h3,h4
(π/2)y
π
τ
τ
1H
13C
Gradient
(π)C1 y
(π)C1 (y+π+φ)
SOSS
U(1,2)
(GPSG)
Detection
Pseudo Hadamard gate

FIG. 5:

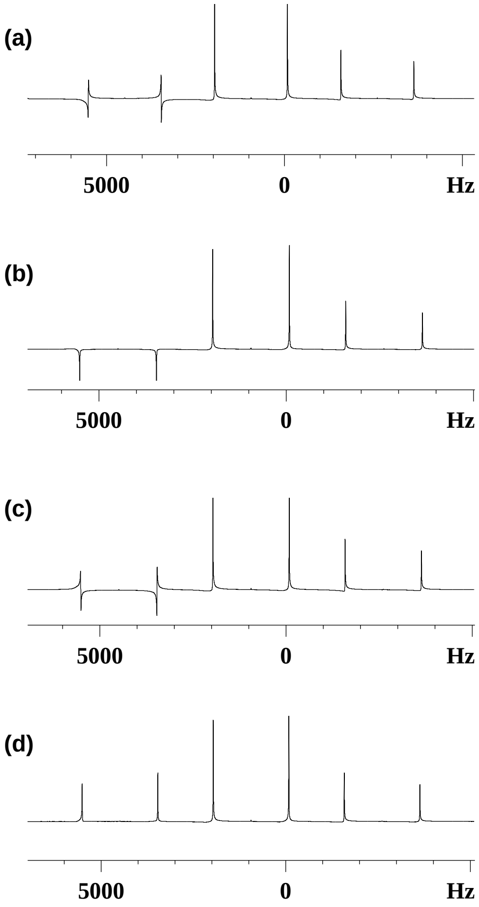

FIG. 6:

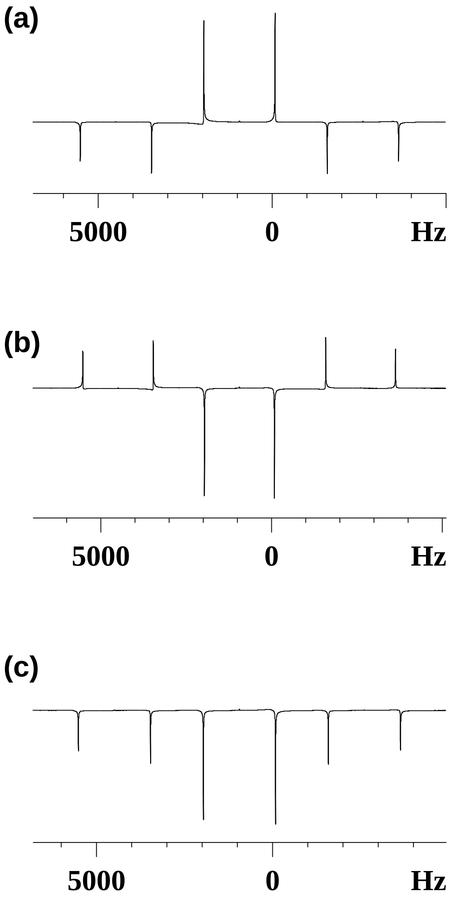

FIG. 7:

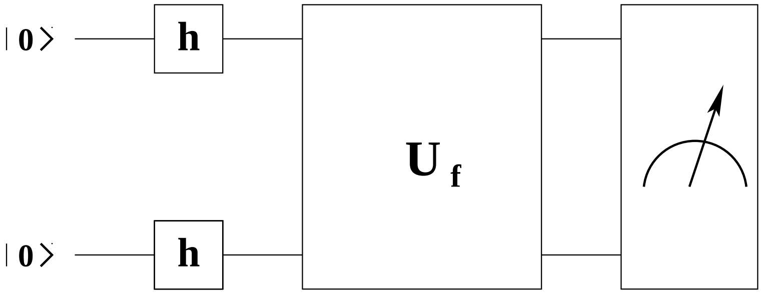

FIG. 8:

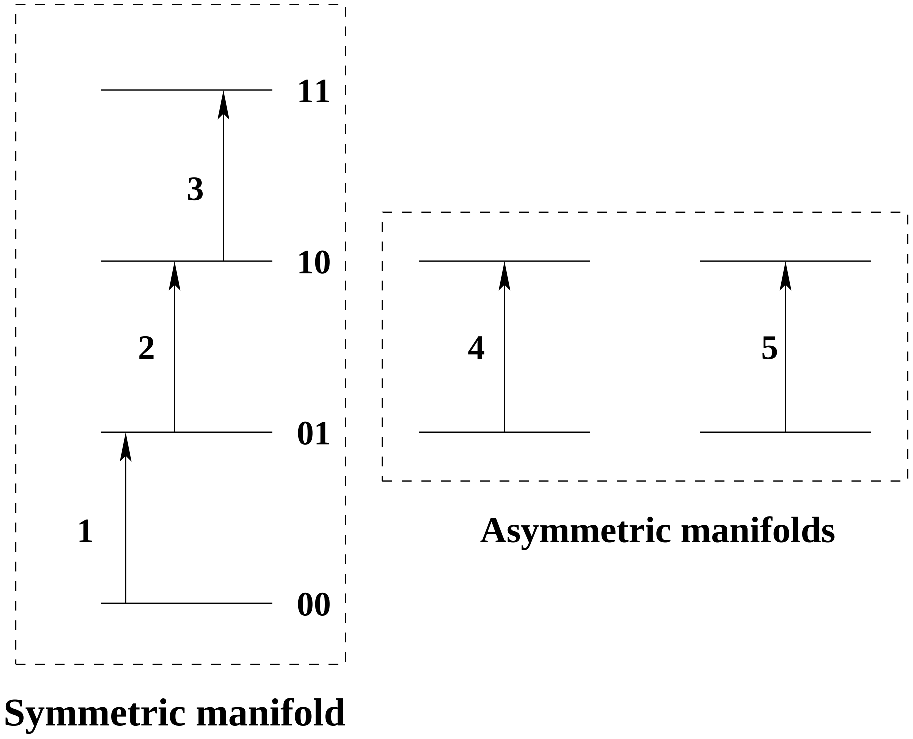

FIG. 9:

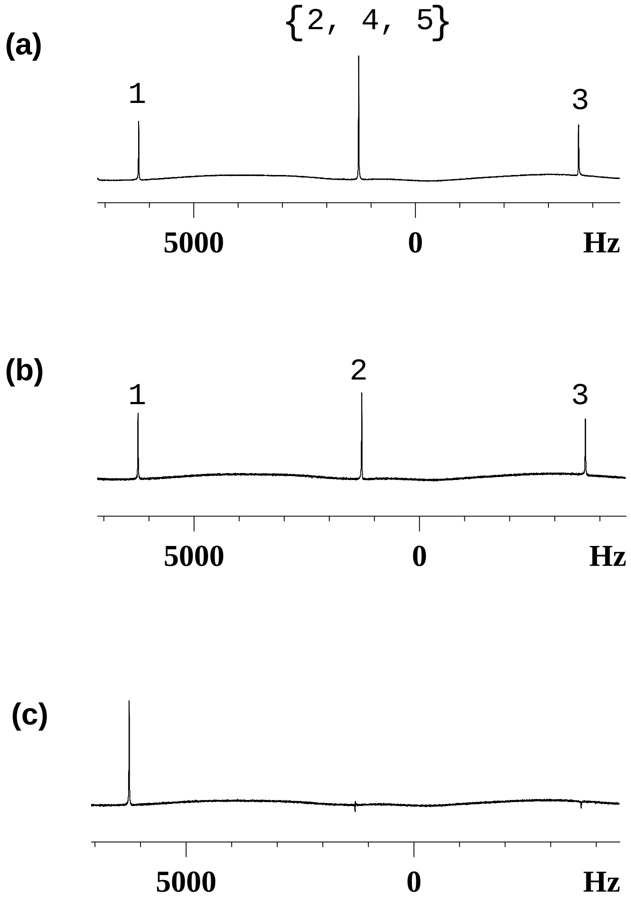

FIG. 10:

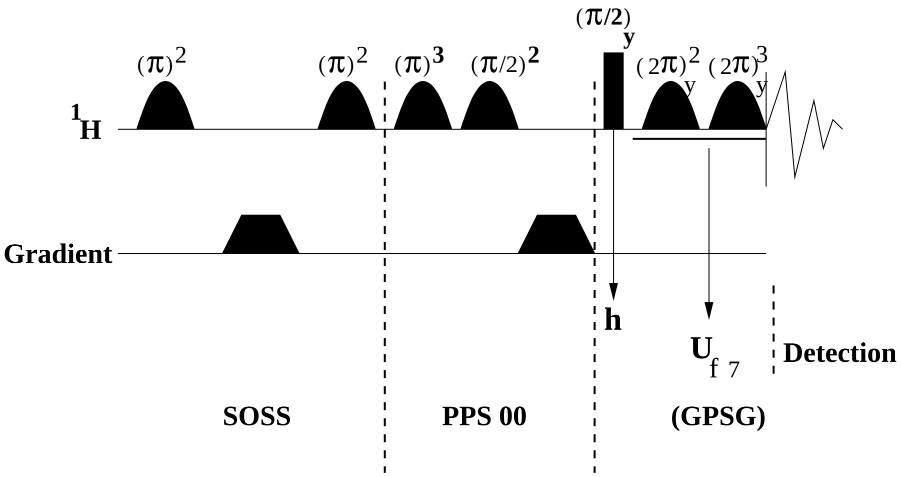
(π)^2
(π)^2
(π)^3
(π/2)^2
(π/2)_y
(2π)^2_y
(2π)^3_y
^1H
Gradient
h
U_f 7
Detection
SOSS
PPS 00
(GPSG)

FIG. 11:

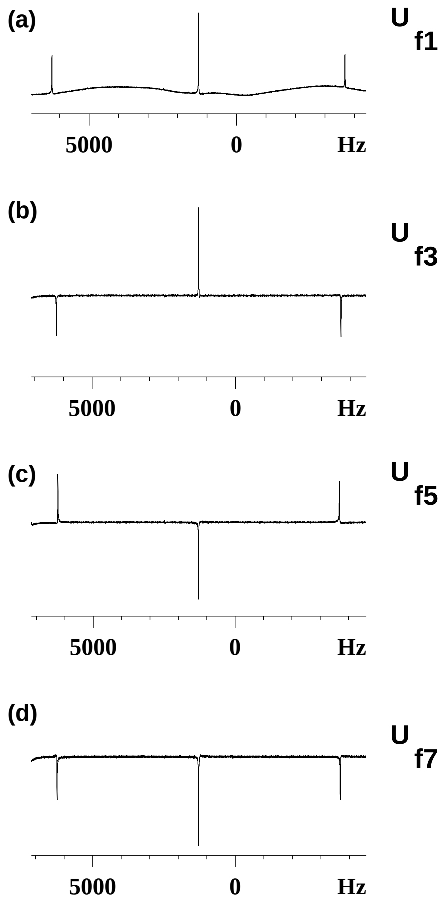

FIG. 12:

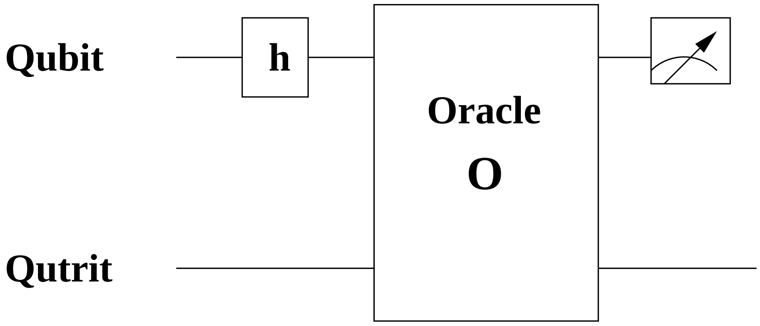

FIG. 13:

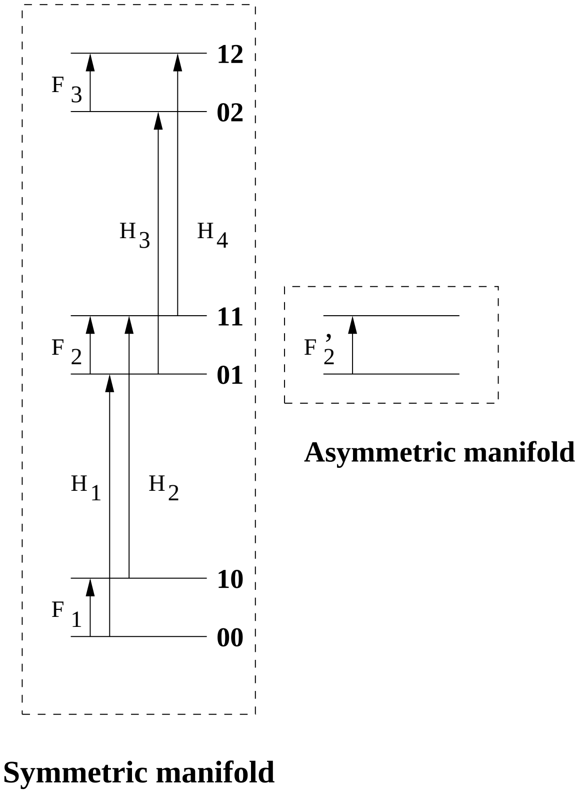
12
F3
02
H3
H4
11
F2
01
F'2
Asymmetric manifold
H1
H2
10
F1
00
Symmetric manifold

FIG. 14:

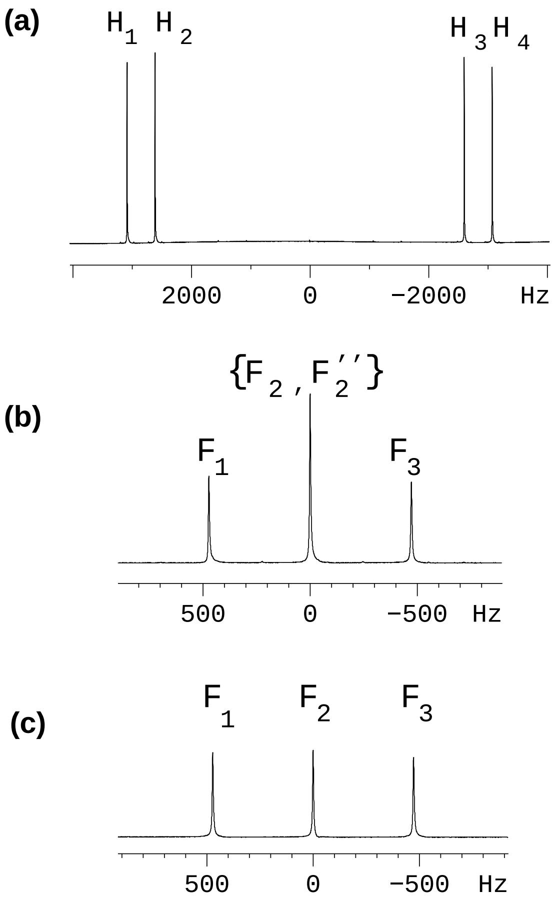
(a)
H1
H2
H3
H4
2000
0
−2000
Hz
(b)
{F2, F2''}
F1
F3
500
0
−500
Hz
(c)
F1
F2
F3
500
0
−500
Hz

FIG. 15:

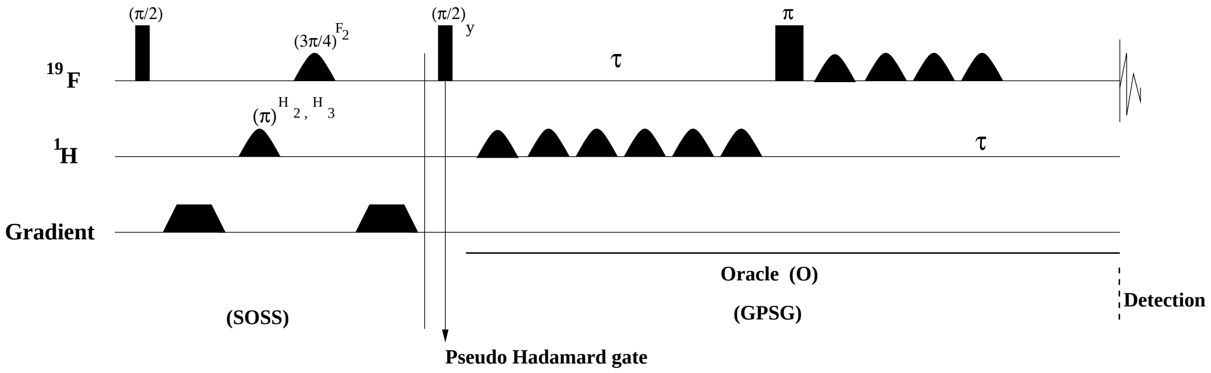
(π/2)
(3π/4)^{F_2}
(π/2)$_y$
π
τ
^{19}F
(π)$^{H_2, H_3}$
^{1}H
τ
Gradient
Oracle (O)
Detection
(SOSS)
(GPSG)
Pseudo Hadamard gate

FIG. 16:

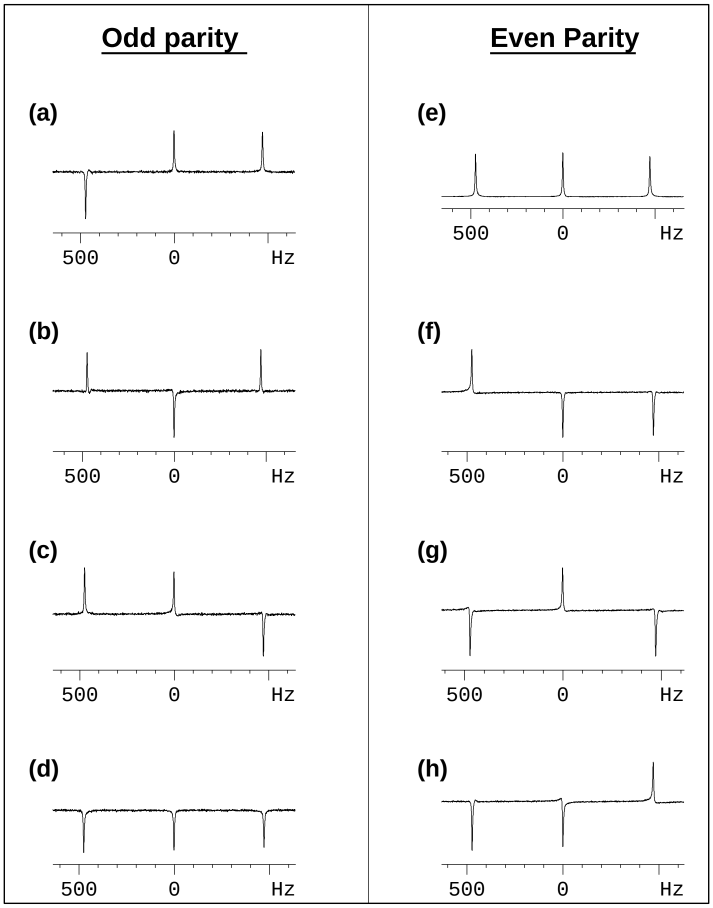

FIG. 17: